Welding in the World
https://doi.org/10.1007/s40194-025-02221-0

RESEARCH PAPER

# Shear force sensors for process monitoring in ultrasonic metal welding—design, calibration, and validation

**Eric Helfers[1] · Oliver Stockemer[2] · Florian Werner Müller[1] · Alexander Schiebahn[1] · Uwe Reisgen[1] · Burkhard Corves[2]**

Received: 11 April 2025 / Accepted: 18 October 2025
© The Author(s) 2025

**Abstract**
Ultrasonic metal welding (USMW) is a widely used solid-state welding process for electrical components. Since the joining zone remains largely hidden during the welding process and high-frequency oscillations are used to form the joint, there is only a limited range of technologies available for process monitoring. The strategies and sensor technologies used so far are not always able to detect process disturbances or defective welds. Consequently, intensive research is currently being carried out to obtain significant process information through additional sensor technology. One solution is to install sensors on the tools (horn and anvil) in the closest distance to the joining zone. Due to their flexibility and contactless measurement, laser vibrometers are frequently used in USMW research to determine the working and interfering frequencies and their amplitudes. However, the integration of such systems into production is limited by the high system costs, the lack of installation space, and the failure of sensors due to contamination. An alternative solution for determining amplitudes and frequencies is the use of piezoelectric shear force sensors in the anvil. This overcomes the challenges of limited installation space and contamination. At the same time, however, sensor integration poses new challenges such as reduced anvil stiffness and possible resonant excitation of the sensor, resulting in a sensor defect. In this study, we demonstrate a design process for a shear force sensor system for USMW, including calibration and validation, which provides high-frequency process information on the anvil side. It is shown in detail that piezo-based force sensors can be used as a cost-effective and integrable alternative to laser-based sensors in USMW processes. The correlation of the measurement data from 175 welding tests results in a mean coefficient of determination $R^2 \sim 0.986$ with an error measure nRMSE of ~ 0.032 between signals of the shear force sensors and a vibrometer as a reference sensor.

**Keywords** Ultrasonic metal welding · Process monitoring · Anvil design · Copper welding · Piezoelectric sensors

## 1 Introduction

Ultrasonic metal welding (USMW) is an industrially established welding process [1, 2]. Although the process is considered the industry standard for some applications, the fundamentals of joint formation and factors influencing the welding process have not yet been fully investigated [3, 4]. As a result, application-specific process development and the assessment of potential errors (i.e., FMEA—Failure Mode and Effects Analysis) repeatedly present challenges. Due to the characteristics of a solid-state welding process, the joint remains covered [3], so that direct process observation and characterization is only possible to a limited extent.

The development of strategies for quality prediction and monitoring has also faced challenges that can only be met to a limited extent with the integrated machine sensor technology used to date. Scalar monitoring of welding time and indentation depth of the horn in an energy-controlled process has been used as standard up to now, but this has proven to be insufficient for recognizing relevant process disturbances [2, 5, 6]. The reasons for this are, on

Recommended for publication by Commission III - Resistance Welding, Solid State Welding, and Allied Joining Process

✉ Eric Helfers
eric.helfers@isf.rwth-aachen.de

[1] Welding and Joining Institute (ISF), RWTH Aachen University, Pontstraße 49, 52062 Aachen, Germany

[2] Institute of Mechanism Theory, Machine Dynamics and Robotics (IGMR), RWTH Aachen University, Eilfschornsteinstraße 18, 52062 Aachen, Germany

Published online: 04 December 2025

the one hand, complex interactions during joint formation and, on the other hand, transient process sequences which are not taken into account in this strategy [1, 3].

Müller et al. [5, 7] have already demonstrated that significantly improved process monitoring is possible by analyzing the mostly available time series data on electrical power and indentation depth. This data has not yet been used for process monitoring or quality prediction in an industrial environment. The analyses carried out show that the quality of data-based models depends not only on the process parameters determined but also on the suitability of the quality indicator or the mechanical testing procedure. This is also evident when analyzing the real joint surface in comparison to mechanical quality tests [8]. A direct transfer of optimized quality prediction models from one application to a new one has not yet been reported [9].

In order to determine significant differences between good and bad welds, research is being carried out into various measurement technologies and strategies [3, 7, 10–12]. The scientists agree that high-frequency information on the amplitude, frequency, and phase characteristics of the tools and weld specimen involved can offer great added value. As part of her dissertation, Balz [3] used laser vibrometers to determine high-frequency amplitude, frequency, and phase curves between the horn, parts to be joined and anvil. Balz was able to successfully demonstrate that the isolated analysis of high-frequency signal components in the range of the excitation frequency and the third higher harmonic (~ 60 kHz) of the working frequency can be used to derive characteristic process curves of Cu-Cu sheet welds. The studies by Gester [12] on wire terminal welds confirm these results. The widespread industrial use of vibrometers in production is limited by their lack of robustness against interference, such as particles in the beam path, and costs. In addition, achieving a good signal as close as possible to the welding process is a challenge; conventional aids such as reflector tape distort the measurement result [13]. Müller et al. [11] and Schwarz et al. [14] have investigated the use of more cost-effective laser triangulation sensors (LTS) as an alternative and have proven their suitability for the application. In their investigations, they were able to identify the vibration amplitude at the anvil as a relevant signal for quality prediction of copper welds, in addition to the power signal and the indentation depth. However, the installation space requirements for LTS, small measuring distance, and the resulting limitations in positioning pose a challenge. Without appropriate efforts to avoid particle contamination of the field of view and the sensor itself, the industrial use of laser-based sensors in ultrasonic metal welding remains problematic, even if purchasing costs continue to decrease and the challenges of installation space are overcome. Other investigations are based on analyzing airborne sound [15, 16] or high-speed imaging [3, 17], while the industrial application of this technologies still faces a number of challenges for USMW.

In conclusion, a technology that can be robustly integrated into the overall welding machine setup is required to record high-frequency USMW process information. One possible technology is the use of piezoelectric sensors. De Vries [6] investigated the use of piezoelectric shear force sensors in the anvil to determine process-relevant information as part of his dissertation and demonstrated their potential suitability for the application. He points out that, assuming the vibration behavior of a simple harmonic motion (undamped single-mass oscillator) for the anvil with a natural frequency $f_0$ of ~ 31 kHz, operation of the sensor system in the subcritical range (working frequency $f < f_0$) is possible, but a significant deviation from real forces is already to be expected when using an excitation frequency of ~ 20 kHz [18]. The system used by de Vries is not calibrated and the available frequency spectrum is not analyzed with corresponding isolation of the relevant signal components. Neither is the mechanical robustness of the measurement setup for a larger number of samples or the correlation to a reference signal presented. In addition, there are also expired patents on the subject of quality monitoring in USMW [19], in particular by integrating an ultrasonic detector in the anvil that is not defined in more detail. The industrial application of such a system has not yet been realized.

As an anvil for USMW should be as rigid as possible while providing high damping [2] so that the highest possible relative movement can be generated between the parts to be joined, a loss of system rigidity due to the use of piezoelectric shear force sensors in the welding process must be critically analyzed if the sensors are mounted in the direct load path. There are already many publications on horn design in general and the working profiles on the horn and anvil [17, 20–22]. However, quantitative and structured studies on the anvil stiffness required for a successful and robust USMW process are lacking, making it challenging to define a corresponding target value.

### 1.1 Summary and research objective

The state-of-the-art shows that acquisition of structure-borne sound in ultrasonic metal welding is a suitable approach to get valuable process data for research on joint formation as well as for setting up predictive quality models. Most sensor methods to determine this information are ill-suited for industrial production environments due to high costs, susceptibility to errors due to dependence on perfect alignment and cleanliness. Using force sensors is an industrially well-suited measuring method compared to other methods, but basic understanding and a thorough validation of the intrusive sensor setup within the anvil are lacking.

The aim of this work is to present and validate a development concept of an anvil for ultrasonic metal welding with integrated, piezo-based shear force sensors. The sensor system is intended to provide high-frequency amplitude and frequency information on the anvil, which can be used for quality monitoring and prediction as well as for process parameterization. The measurement data should be usable not only qualitatively but also quantitatively. The concept consists of the CAE-supported design process, implementation and calibration as well as validation using a data set of 175 welding experiments.

## 2 Methodology and experimental setup

The anvil with integrated shear force sensors is intended to be used in a larger test setup for USMW. The basis is an industrially used Schunk LS-C welding machine with 4-kW generator power. An application-specific horn with a square working surface of 5 mm × 5 mm and a diagonal knurl pattern in the form of a truncated pyramid (0.8 mm × 90°, flattened by 0.1 mm) is used. The application-specific, exchangeable anvil element has a working surface of 10 mm × 10 mm with a diagonally arranged, pyramid-shaped knurl pattern (0.5 mm × 90°). Sheets of electrolytic tough pitch cold-rolled copper strip—Cu-ETP [23]—with a thickness of 1 mm and 60 mm × 30 mm (length × width) are welded in an overlapping arrangement. The upper and lower part are each positioned using a steel positioning mask and clamped pneumatically with ~ 500 N force. The test setup and the specimen geometry are shown in Fig. 1 and Fig. 2. Since there is no standardized reference sample for USMW of sheet metal or busbar joints, the component geometry was selected so that reasonable testing in a shear tensile test was possible. For this reason, the sheet cross-section (30 $mm^2$) was chosen to be larger than the joint cross-section (25 $mm^2$).

The experiments in this study are each welded with the same set of welding parameters (see Table 1) in an energy-controlled process. The welding parameters were optimized prior to the study with statistical methods (DoE—design of experiments) for the reference condition (*R*).

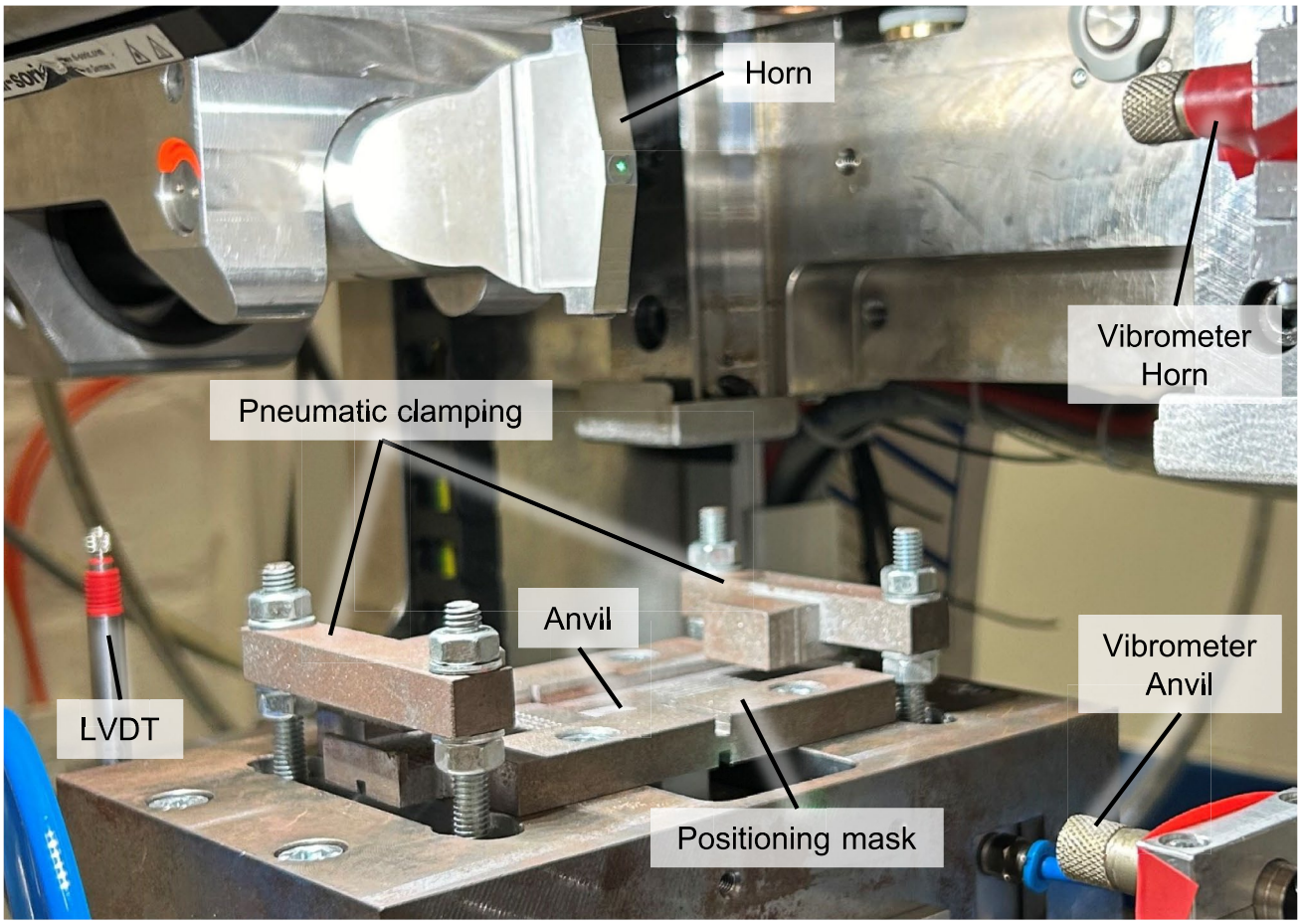



**Fig. 1** Welding setup with welding tools, clamping arrangement, and external sensors

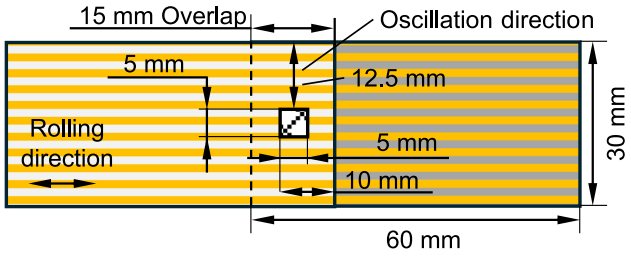



**Fig. 2** Schematic representation of the specimen geometry (thickness $t = 1$ mm)

**Table 1** Welding parameters—original parameters and machine settings in brackets

| Parameter | Value |
|---|---|
| Force | 625 N (1.25 bar) |
| Amplitude | 30 µm (110%) |
| Energy | 1600 J (1600 Ws) |

Target values for the DoE were a maximum tensile shear force and an indentation depth of ~ 0.3 mm—0.35 mm. The nominal amplitude of 30 µm is achieved in idle oscillation without component damping at the middle of the horn, as depicted in Fig. 1.

One hundred seventy-five welding experiments were carried out to validate the developed shear force sensor setup. In addition to the reference setup (*R*), four deviating variants are prepared, each with 35 samples. The reference setup consists of copper sheets with a specified tensile strength ($R_M$) of 240 MPa (R240) and a part surface which is not cleaned (EXW – ex works) any further after removing the protective polyethylene film directly before welding. The samples in test series C (chemically cleaned) are cleaned in an ultrasonic bath for five minutes with the solvent 2-propanol. After cleaning, the solvent evaporates in the ambient air. In addition, a copper sheet with higher specified strength and hardness (H) due to higher work hardening, a condition with contamination (*F*) by diluted rolling/sliding bearing grease (1 part Klüber Microlube GNY 202: 100 parts isobutanol) and a condition without pneumatic clamping of the sheets (X) are analyzed. Table 2 provides a concise overview of the sample variations.

## 2.1 Anvil design

The design process of the anvil goes through three steps, which are iterative rather than consecutive, until the defined requirements are met. Before the beginning of the design process, some requirements are defined:

- It should be possible to change the working surface of the anvil, prone to wear, without having to recalibrate the measurement system. For this reason, a test platform should be created on which an anvil element can be mounted.
- The design should be carried out with sufficient distance to critical natural frequencies so that a possible resulting sensor defect is avoided. The largest shear force sensors currently available on the market—HBK CSW/8kN—[24] are intended to be used in order to minimize the expected loss of stiffness of the anvil.

### 2.1.1 Single mass oscillator

At the beginning (1st step), the anvil and shear force sensors are simplified as a single-mass oscillator [25]. It quickly becomes evident that subcritical operation ($f \ll f_0$) or design in this range is not possible if the sensor manufacturer's design specifications are to be met [24]. De Vries [6] achieved a natural frequency of ~ 31 kHz for his shear force measurement setup, neglecting design constraints as specified by the sensor manufacturer. The use of piezoelectric sensors above the system's natural frequency (assembly consisting of sensor and structure) is generally not recommended, as the sensors have very low damping due to the materials used [26]. If a piezoelectric force sensor is nevertheless to be operated above the natural frequency of the measurement setup in load path, the following must be considered:

- Linear transfer behavior can no longer be assumed in general [26]. The transfer behavior must be checked on a case-by-case assessment.
- If the natural frequency of the overall system is passed through during operation, there is not only a risk of destruction of the overall system [18], but also of the

**Table 2** Overview of the weld specimen configurations

| Test series | Additional information | Base material | Cleaning | Contamination Diluted oil | Number of welds |
|---|---|---|---|---|---|
| R | Reference (foil clean) | Cu-ETP R240 | - | EXW | 35 |
| C | Chemically cleaned | Cu-ETP R240 | 2-Propanol | - | 35 |
| H | Hardness | Cu-ETP R290 | - | EXW | 35 |
| F | Contamination | Cu-ETP R240 | - | 1:100 | 35 |
| X | Without clamping | Cu-ETP R240 | - | EXW | 35 |

sensor itself if the overall system has a similarly low damping as the sensor (resonance failure).
- The natural frequency should be passed through as quickly as possible (short load duration) and with the lowest possible excitation amplitude.
- A sufficient frequency spacing between the system's natural frequency and the operating frequency should be guaranteed.

The advantage of USMW is that the operating frequency is not achieved by a classic "ramp-up" of the system, like the acceleration of a shaft or a washing drum. This means that "only" the investigation of the transfer behavior and a sufficient frequency distance to critical system natural frequencies remain as steps for the dynamic design of the anvil system. It was not possible to determine literature values for an adequate distance to critical natural frequencies for anvils, whereas a minimum distance of ~ 1000 Hz is usually specified for horns [20]. The specification of the critical natural frequencies for the horn refers to unwanted vibration modes such as bending modes, which must have a certain minimum distance to the operating frequency range. In the first iteration step (see Fig. 3), it is therefore assumed that the resonant frequency $f_0$ of the anvil structure must be less than ~ 14,150 Hz in order to fulfill the target of amplitude transmissibility $V \leq 1$ at welding frequency of ~ 20 kHz (frequency ratio $\frac{f}{f_0} > \sqrt{2}$). Independent of the occurring damping coefficient $D$, no further gain in amplitude can be expected at this frequency ratio. A closer look at the phase shift between the excitation and the system motion in the x-direction (Fig. 3) shows that the phase behavior in the design area is highly dependent on the actual damping and the frequency ratio.

Since data sheet of the shear force sensors only provides information to calculate a shear stiffness value $c_{Shear}$ in unmounted state, a deviation in the range of ± 20 % must be assumed when designing the system in the assembled state [27]. The mass of the anvil is assumed to be $m_{Anvil} = 0.61\ kg$ for simplicity, by extracting it from the CAD model. Assuming the specified boundary conditions, the requirement of $V \leq 1$ is met with $f_0$ of the anvil system between ~ 10,871 and 13,314 Hz. The corresponding assumptions are shown in Fig. 3.

### 2.1.2 Harmonic analysis

Since the assumption of the entire system as a single-mass oscillator offers a high potential for errors and the anvil hardly behaves like a rigid body, a harmonic analysis of the system (finite-element-method—FEM) was also carried out (2nd step). To perform the harmonic analysis, assumptions

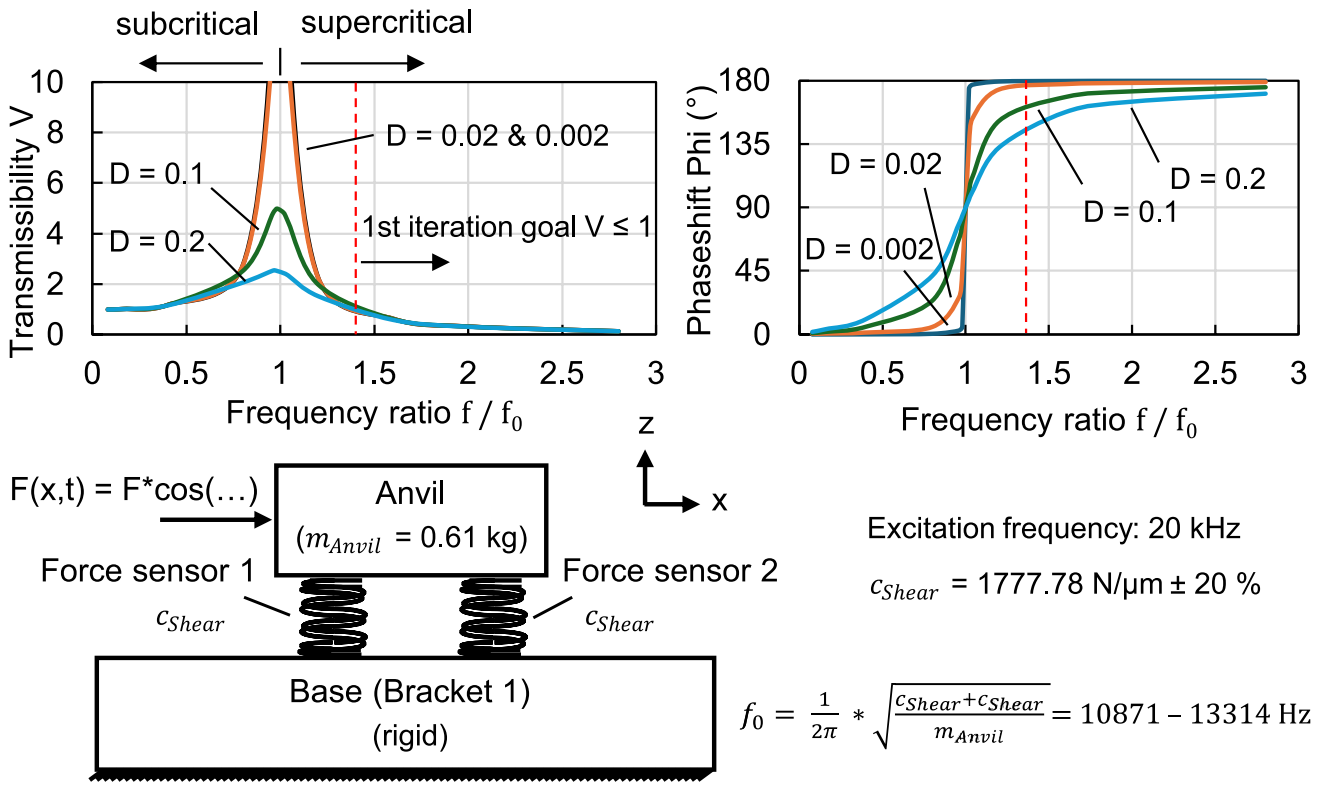



**Fig. 3** Anvil with two integrated shear force sensors as a simplified model of a single mass oscillator with harmonic force excitation

are made regarding the material properties of the components involved. The material data of the metallic materials used are taken from literature [28]. The properties of the piezoelectric ceramic including the steel housing are determined and tuned by means of a modal analysis (FEM) of a sensor dummy with the geometric dimensions of the sensor, so that the natural frequency according to the data sheet is achieved. The assumed material properties are summarized in Table 3.

In particular, estimating the damping in the tools during ultrasonic welding is challenging because it depends on the applied material stress, frequency, component geometry, and the material properties. Since the anvil construction consists of a material combination (steel/cast iron), an average loss factor of $\eta \sim 0.02$ ($\eta = 2 * D$) can be assumed for the entire construction based on literature data [25, 29, 30] for damping. The assumptions in simulation must then be validated experimentally. The simulation is carried out with Ansys Workbench R2021 with the full matrix method in three configurations with a variation of $\eta$ between 0.002 and 0.04. The loss factor is not adjusted depending on the component.

The shear force sensors are simplified as homogeneous objects with isotropic material properties. The anvil structure is firmly clamped on the bottom side. A harmonic excitation with an amplitude of 8.5 µm is applied to the top surface, where the lower joining part is positioned in reality. The test setup is shown in Fig. 4. In addition, Fig. 4 shows the measuring point used for the vibrometer in experimental analysis and validation.

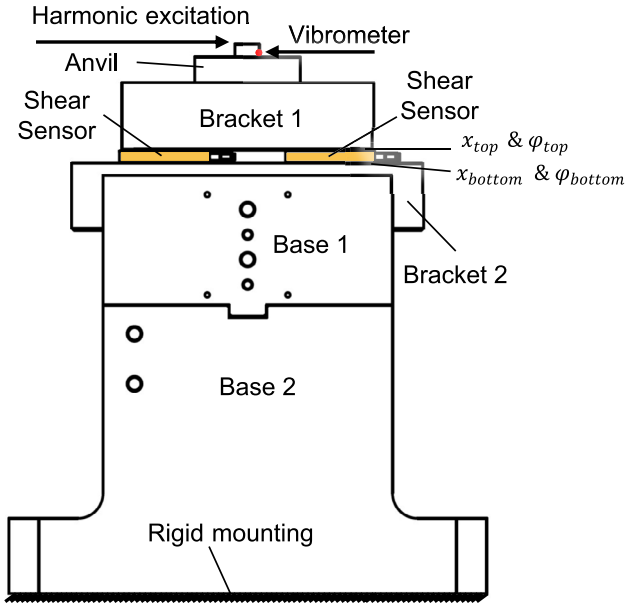



**Fig. 4** Test setup in Ansys Workbench R2021 for harmonic analysis

The differential frequency response between the top ($x_{top}, \varphi_{top}$) and bottom ($x_{bottom}, \varphi_{bottom}$) side of a shear force sensor in direction of excitation is then formed. The mean amplitude peak value $x_{res}$ as a function of the respective phase angle $\varphi_i$ for the excitation is obtained as follows:

$$x_{res} = \sqrt{x_{top}^2 + x_{bottom}^2 - 2x_{top}x_{bottom}\cos\left(\varphi_{top} - \varphi_{bottom}\right)} \;\&\; \varphi_{res} = \varphi_{top} - \varphi_{bottom}$$

The results for amplitude and phase response are shown in Fig. 5. Between 1000 and 25,000 Hz, there are a large number of resonant modes in load direction. Below 1000 Hz, no further natural frequencies of the system are found and there is no further relevant reduction in the amplitudes. The maximum displacement $x_{res}$ between the top and bottom of the sensor is achieved at 7680 Hz with around 58 µm at $\eta \sim 0.002$. At this frequency, the entire anvil structure vibrates in the direction of excitation. Starting at a loss factor of 0.02, the maximum displacement of > 11 µm occurs at ~ 11,800 Hz. The shear force sensors and the structure above them are excited with the highest intensity in this situation. If the phase behavior of the top and bottom side of the sensor is considered individually for the excitation, it becomes clear that the anvil structure behaves like a coupled multi-mass oscillator. Starting at an excitation frequency of ~ 14,200 Hz, a phase of more than 180° can be detected between the excitation and the bottom side of the sensor. At about 15,080 Hz, a bending mode of the structure occurs. Above this frequency, the system is primarily excited to more complex mode shapes and higher-order modes. It was

**Table 3** Material data for harmonic analysis of the shear force measurement setup

| Component | Material | Young's modulus E [GPa] | Poisson's ratio $\nu$ [-] | Specific mass $\rho$ [g/cm$^3$] |
|---|---|---|---|---|
| Anvil | Cold work tool steel | 218 | 0.285 | 7.68 |
| Bracket 1 and 2 | S355J2+N | 212 | 0.285 | 7.85 |
| Shear sensor | Piezoceramics/steel housing | 79 | 0.33 | 7.7 |
| Base 1 and 2 | GJS-500-7 | 169 | 0.275 | 7.1 |

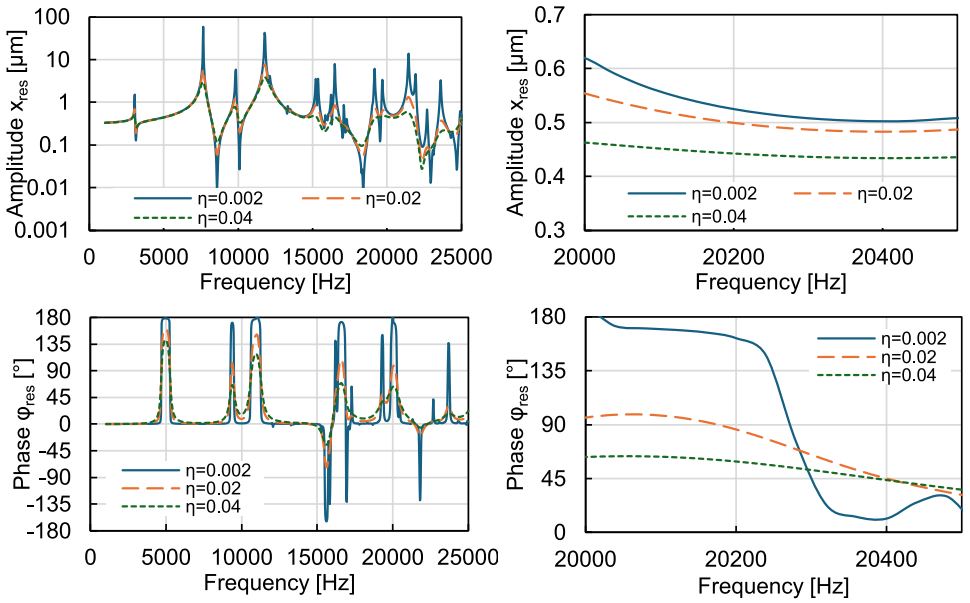



**Fig. 5** Harmonic analysis—amplitude and phase response (x-direction) of one shear force sensor for harmonic excitation with 8.5 µm amplitude—left side: 1000–25,000 Hz, right side: detailed view 20,000–20,500 Hz

found that the achieved amplitude at the anvil, especially in the working range between ~ 20,000 and 20,500 Hz, depends significantly on the assumed loss factor and, as a result, the present damping. In particular, with a loss factor of 0.02 for the amplitude between 20,100 and 20,500 Hz the change in amplification is very low. The phase response $\varphi_{res}$ in the frequency range 20,000–20,500 Hz is also heavily dependent on the damping and ranges between 0° and 180°.

When comparing the present amplitudes at the input frequency of 1000 Hz and 20,200 Hz, a transmissibility in the range ~ 1.34–1.59 between the top and bottom of the piezoelectric sensor can be observed, depending on the present loss factor. The resulting amplitudes and associated assumptions are summarized in Table 4. A corresponding increase in the measurement signal must therefore also be expected in the real application. Furthermore, the real amplitude gain can only be determined in advance by simulation if highly accurate material parameters are available for all the components involved as a function of the stress. This data is not yet available.

#### 2.1.3 Static-mechanical analysis (FEM)

At last (3rd step), the anvil structure is subjected to a static-mechanical analysis (FEM) and the result is compared with the available deflections in the harmonically excited state. For that purpose, the base is clamped firmly in the model and a force of 1000 N is applied to the center point of the anvil's work surface, followed by a force of 2500 N in a second simulation (see Fig. 6). Consequently, a maximum mechanical deformation of ~ 3.5 µm at 1000 N and ~ 8.5 µm in the x-direction occurs at the work surface (point 1). Figure 6 shows that more than 70 % of the deformation results from the anvil structure above the shear force sensors. The shear force sensors thus have a significant influence on the system stiffness, but at the same time they are not the decisive element for the resulting total deformation in load direction. Between the top and bottom of a shear force sensor, a deformation of ~ 0.16 µm at 1000 N and ~ 0.4 µm at 2500 N in x-direction occurs.

Based on the calculations and analyzes carried out, the shear force sensors can be expected to operate in a functional and robust manner since the amplitudes present are within the sensor's operating range ($x_{res} < S_{nom} \sim 4.5\ \mu m$) and critical resonant modes are only present at a sufficient distance from the working frequency.

### 2.2 Data collection and analysis

A system for high-frequency, simultaneous data recording is used for calibration and validation of the shear force sensor setup, the measurement chain is depicted in Fig. 7.

A data acquisition system from National Instruments Corporation with 500 kS/s (simultaneous) measuring rate per

**Table 4** Amplitude gain between top and bottom of one piezoelectric shear sensor as a function of damping when excited with 8.5 µm amplitude

| | Loss factor η = 0.002 | Loss factor η = 0.02 | Loss factor η = 0.04 |
|---|---|---|---|
| Magnitude @ 1000 Hz | 0.33 µm | 0.33 µm | 0.33 µm |
| Magnitude @ 20,200 Hz | 0.525 µm | 0.499 µm | 0.443 µm |
| **Transmissibility V** | **1.59** | **1.51** | **1.34** |

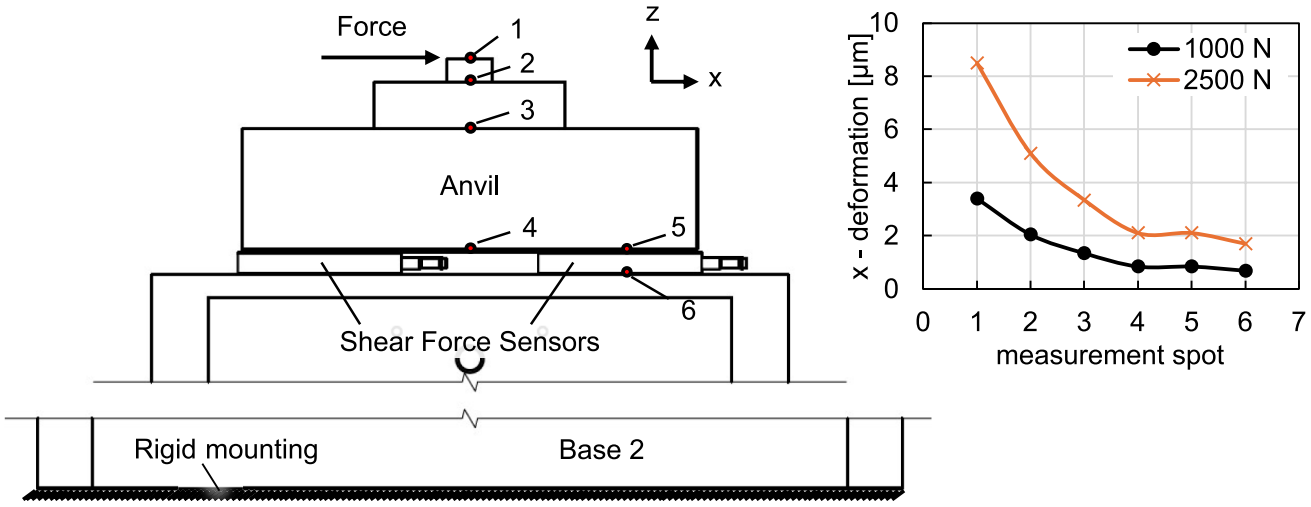



**Fig. 6** Mechanical deformation of the anvil structure due to static load (FEM simulation Ansys)

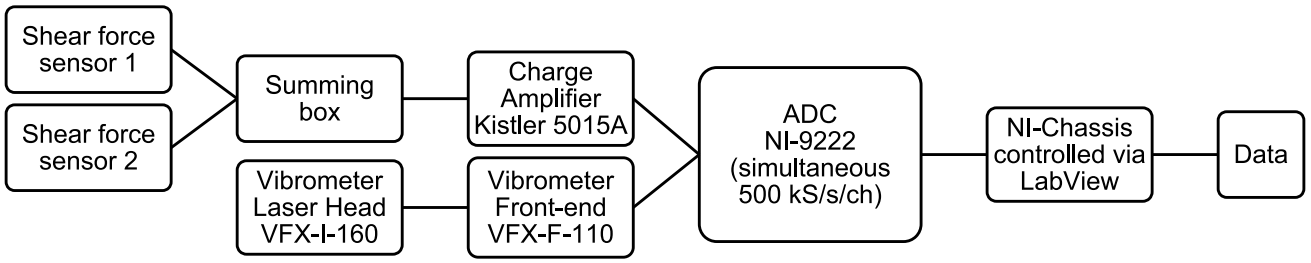



**Fig. 7** Measurement chain for shear force and vibrometer data

channel is used for voltage signal acquisition and digitization. The piezo electric shear force sensors are connected to a summing box. The common signal, still a charge signal, is converted to a voltage signal, proportional to the load, by a Kistler 5015 A laboratory charge amplifier. A 1D laser vibrometer from Polytec—VibroFlex QTec VFX-I-160—is used at the anvil as a reference signal during the welding experiments to validate the data obtained from the shear force sensors.

In addition, four further fully synchronized measurement signals are recorded for process analysis using an additional NI-9222 module. For this purpose, another vibrometer—a Polytec VibroFlex Xtra VFX-I-120—is used on the horn, and the electrical power signal of the ultrasonic generator, a linear variable differential transformer (LVDT) for the indentation depth and a normal force sensor in the piston rod of the pneumatic cylinder are acquired.

## 3 Results and discussion

In addition to the calibration and validation process for the shear force sensors, exemplary signal curves for the welding power, indentation depth, and vibrometer signal at the anvil are presented below. Furthermore, some statistical parameters and the results of the mechanical testing of all samples are presented to confirm that the welds are a representative sample.

### 3.1 Force sensor calibration

Piezoelectric force sensors are usually used in a preloaded and mounted state within an application. This causes the sensitivity of the sensor to decrease compared to the specified value in the data sheet, and the sensor must be calibrated [24]. Specifically, the gain of the charge amplifier or the conversion factor in the measurement data acquisition is adjusted. The shear force sensor setup is calibrated using a reference measuring system, a universal testing machine. The procedure used is the so-called 2-point calibration in

a quasi-static state. The range of interest is defined by an upper and a lower value. Subsequently, linear transmission behavior is assumed between those points, defining the range of interest. The process of two-point calibration is shown in Fig. 8. For calibration, a force of 1000 N and 2500 N is quasi-statically applied to the sensor setup twice.

Before calibration, an average sensitivity of 8.24 pC/N was used, which was calculated as the mean value from both sensor data sheets. The corrected sensitivity of 7.7 pC/N can subsequently be calculated from the deviation of the force determined between the reference sensor (Zwick Z5.0 testing machine) and the shear force sensor, which corresponds to a reduction of ~ 6.6 %. The experimental setup for the calibration is shown in Fig. 9.

### 3.2 Welding results

The welding tests are described below, the data from which will later be used to validate the shear force measurement setup using the vibrometer signals. Table 5 shows the major statistical values of the welding experiments carried out. After each weld, the sample was mechanically tested to determine weld quality by means of quasi-static tensile shear testing. For all test series, the mean values and standard deviations were determined for the welding time achieved, the indentation depth and the maximum shear tensile force. Depending on the test series, the welding time is on average between ~ 740 ms – 1130 ms, with a standard deviation of ~ 3.7 – 9.3 %. The mean indentation depth is within ~ 0.21 – 0.4 mm with a standard deviation of ~ 6.8 – 14 %. The mean maximum tensile shear force is between ~ 2177 – 3157 N with a standard deviation of ~ 4.2 – 11.6 %. In test series X, there is a single significant negative outlier with a determined maximum shear force of only 1238 N.

In addition to the solely scalar evaluation of the welding time and the maximum indentation depth, further process information can be determined from the time curves of

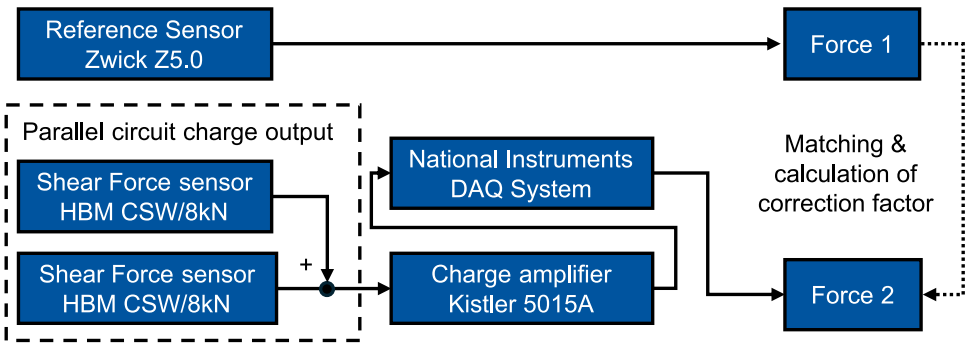



**Fig. 8** Two-point calibration procedure

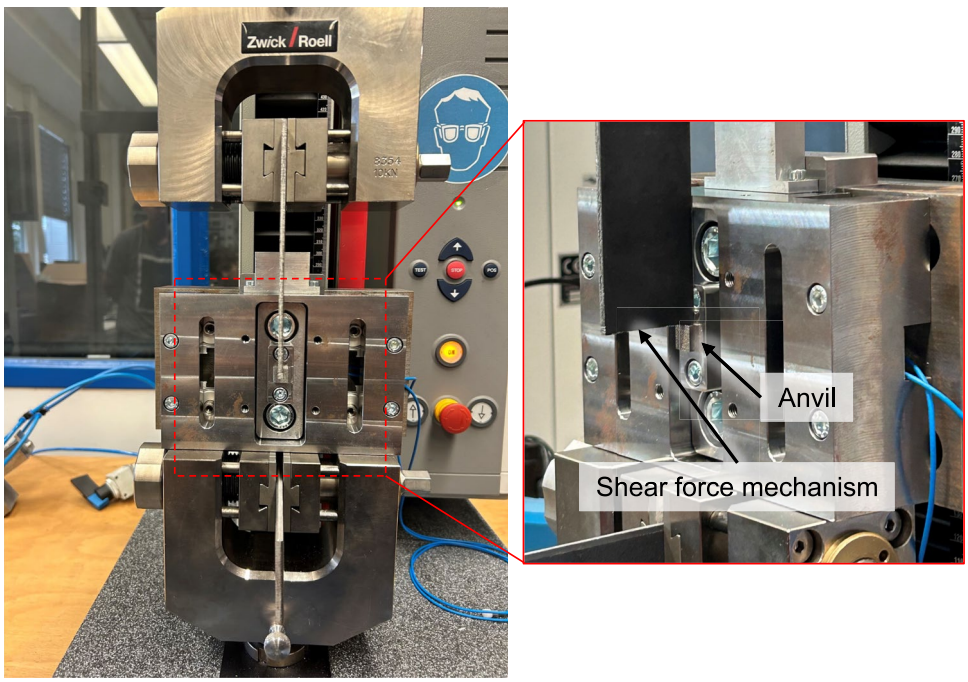



**Fig. 9** Test setup for calibrating the shear force sensors with reference system

welding power and indentation depth, as described in the literature [7, 11]. Figure 10 shows an example of a characteristic process curve for each of the test series, the maximum tensile force determined is highlighted in color. Their algorithm-based evaluation usually allows a clear distinction between different conditions and a quality prediction [5], whereby even a simple observation provides some information. The significantly increased welding time in test series X, for example, results from the significantly lower power compared to the other test series starting at ~ 100 ms. This is attributed to the missing sample clamping and the lower plastic deformation of the sheets, which results from the reduced indentation. In addition, the upper sheet performs a plane bending (natural frequency) mode without being clamped, which needs less power. The power curves of R, C, and H are largely comparable, with the indentation differing primarily due to a significant spread at the end of the weld. The power curve of F shows a second significant increase from ~ 400 to 450 ms into the weld, with a simultaneous sharp increase in the indentation depth.

However, detailed information on the forces acting and resulting amplitudes on the anvil is still missing. By exemplary evaluation of the vibrometer signals measured at the anvil and the shear force signals by bandpass filtering (19 – 21 kHz) and envelope detection via Hilbert transform, a good correlation of the two signals can be seen (see Fig. 11). Compared to the power and indentation signals, all curves for anvil amplitude and shear force show an initial steep increase with a first level followed by a second steep increase with a degressive curve afterwards until the end of the weld, which is consistent with the studies by Balz and Gester [3, 12]. In test series F, the second shear force level

**Table 5** Statistical overview of the welding results of the five-test series

| Test series | Mean welding time | Std. dev. of welding time | Mean indentation depth | Std. dev. of ind. depth | Maximum shear force (mean) | Std. dev. of force |
|---|---|---|---|---|---|---|
| | [ms] | [%] | [mm] | [%] | [N] | [%] |
| R | 776.97 | 9.34 | 0.35 | 13.98 | 2676.04 | 7.78 |
| C | 737.50 | 5.86 | 0.39 | 11.44 | 2634.57 | 8.42 |
| H | 757.09 | 5.13 | 0.30 | 14.66 | 3156.84 | 4.23 |
| F | 792.26 | 3.65 | 0.40 | 10.64 | 2399.75 | 8.19 |
| X | 1129.40 | 8.43 | 0.21 | 6.80 | 2176.50 | 11.62 |

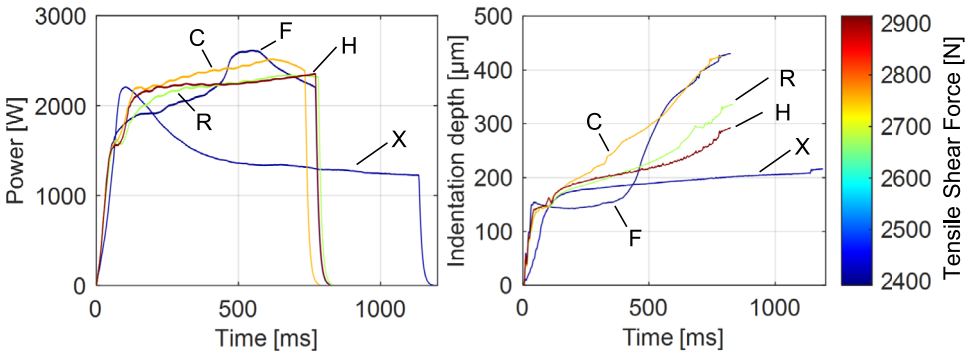



**Fig. 10** Exemplary curves of power and indentation depth for one weld of each test series

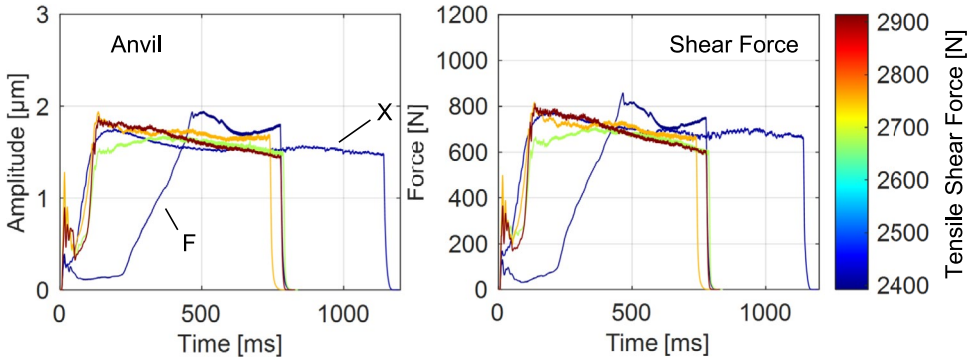



**Fig. 11** Exemplary curve of vibrometer signal at the anvil (left) and shear force sensors (right), each of a weld per test series

is only reached after about 450 ms, which is achieved in the other test series after ~ 100 ms. The reduced friction coefficient due to contamination with oil significantly reduces the forces transmitted to the anvil until it is pushed out of the joining zone. Without a detailed analysis of the power and displacement signals or additional process information at the anvil, the disturbance with organic contamination would not be detectable. However, industrial application of an additional signal at the anvil is only of interest if a robust correlation can be achieved for a large data set.

### 3.3 Force sensor validation

To evaluate the quality of the shear force sensor setup and measurements, a process for the detailed, automated correlation of vibrometer and shear force data is presented below. To validate the results of the shear force sensor setup, the correlation of this signal with the vibrometer signal measuring the anvil oscillation is analyzed. This requires some pre-processing of the raw data to obtain meaningful results. For machine learning for weld quality prediction as well as investigations on the joint formation and other evaluations, analysis of the envelope curves of the time series have proven to be of great importance [3, 11, 12]. The use of amplitude envelopes instead of the raw signal reduces the computational effort significantly.

To compare the signals, they are standardized to the minimum and maximum values of each signal. Other more complex algorithms, such as the *Standardscaler* of the scikit-learn library [31] in Python, provide even better results for the coefficient of determination $R^2$, but at the cost of worse results for the normalized root-mean-squared-error (nRMSE).

The unfiltered, noisy signal from both sensors for an exemplary weld belonging to the group of the reference welds (*R*) is shown in Fig. 12 (left). During this weld, shear forces up to 1500 N and anvil velocities at the measurement point of 0.8 m/s were achieved. Figure 12 (right) depicts the bandpass filtered signals.

Analogue to the analysis of the raw signal in the time domain, the signal composition can be compared in the frequency domain. Figure 13 shows the two power spectrums derived using a Fast Fourier Transform of the sensor signals.

The peak values of the two signals with correspondingly pronounced frequencies are close to each other, the background noise between these values differs more strongly. The welding frequency of 20 kHz (b)) as well as the higher harmonics at 40 kHz (c)) and 60 kHz (d)) can be clearly identified. The peaks at the second higher harmonic differ slightly compared to the other peaks, with the vibrometer signal being 20 dB lower than the shear force signal. Due to the comparatively high signal-to-noise ratio, analyzing the

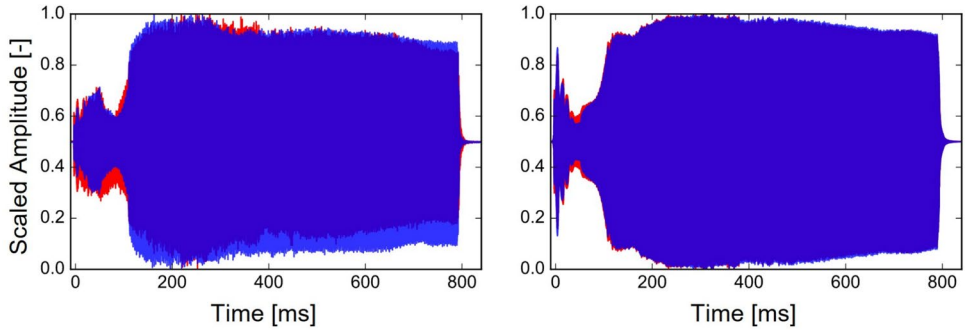



**Fig. 12** Standardized signals of shear force sensor (red) and vibrometer sensor (blue); left: raw signals; right: bandpass-filtered signals

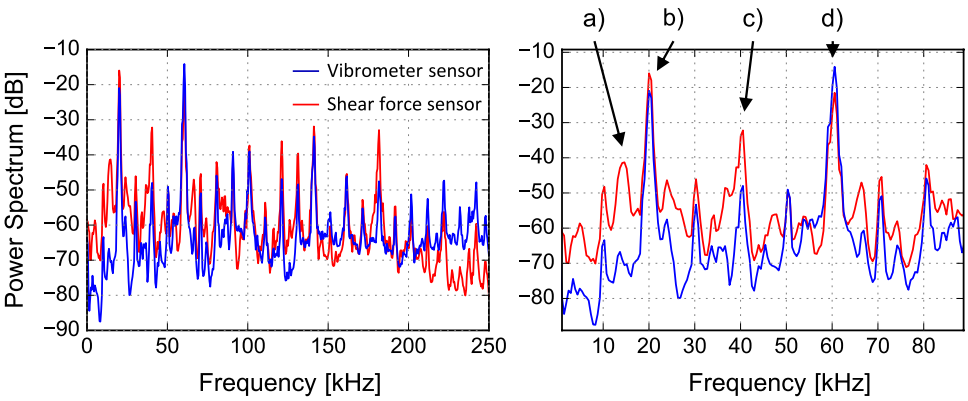



**Fig. 13** Power spectrum of the standardized signals of shear force sensor (red) and vibrometer sensor (blue); left: complete frequency range; right: detailed view of 0 to 90 kHz; **a** natural anvil resonance frequency (~ 14.3 kHz); **b** response to excitation frequency; **c** 2nd higher harmonic (~ 40 kHz); **d** 3rd higher harmonic (~ 60 kHz)

operating frequency and its harmonic multiples is sufficient for validating the measurement method.

The first step in data processing is to extract the signals at these relevant frequency ranges. The most important is the operating frequency at about 20 kHz. In addition, the behavior of the system at the higher harmonics at 40 kHz and 60 kHz is validated. A bandpass filter (5th order Butterworth filter) is used to extract the signals in the frequency ranges. A filter bandwidth of 1000 Hz, i.e., from 20 to 21 kHz, is selected. This results in the filtered signal shown in Fig. 12 (right), which shows a high correlation between the shear force sensor signal and the vibrometer signal. In this frequency range, shear forces up to 700 N and anvil velocities at the measurement point of 0.2 m/s were achieved. Selecting a wider bandwidth will slightly degrade the results. Only simple bandpass filters are used in this paper. Other filter systems such as wavelets or synchro-squeezed wavelet transforms have been used in analysis of USMW and seem to give similar or better results but tend to be more computationally expensive [11, 32]. Future work will analyze whether using such methods results in significant differences for the evaluation of the shear force signal.

As the next step in data preprocessing, the envelope curves of the amplitudes in the distinctive frequency ranges are extracted from the filtered signals using the Hilbert transform.

Since the filtered band width is still quite large at 1000 Hz, there is still room for interfering frequencies in the signal up to 1000 Hz. One of the main interfering frequencies is at 300 Hz, which appears as a beat frequency in the signal and is caused by the welding machine itself. To get rid of this frequency, the determined envelopes are low-pass filtered with a cutoff frequency of 200 Hz. Since the envelopes no longer contain the high-frequency oscillations, a sampling rate of 500 kS/s is no longer required. Therefore, the signals are down sampled to a sampling rate of 1000 S/s. The result of the processing is shown in Fig. 14. It shows the best and worst results of the correlation analysis of the two sensor signals.

The beginning of the process is characterized by a steep slope in the measured signals, which both sensor signals represent very well and consistently. At the following amplitude drop, some differences in the signals can be seen. In the final phase of the process, with more constant amplitudes, most of the signals show a high correlation with almost no deviations in the two signals (as in the left one). However, some signals seem to have a slight offset that remains more or less constant in the final phase of the welding process (like the one on the right). This can be caused by various reasons, besides the obvious difference that the measuring points are in two different locations: charge losses or interference charges in the piezoelectric measuring chain, amplification errors in the charge amplifier, mechanical overloading of the sensor or mechanically complex movement in the anvil. These possible causes still need to be investigated in detail.

Various parameters are used to objectively evaluate the accuracy of the time signals between the shear force sensor and the vibrometer signal. The normalized root-mean-square error (nRMSE) provides information about the deviation of the two signals and is calculated as follows:

$$nRMSE = \frac{1}{y_{max} - y_{min}} \sqrt{\frac{1}{n} \sum_{i=1}^{n} (y_{shear} - y_{vibro})^2}$$

In addition, the coefficient of determination $R^2$ is used to evaluate the correlation of deflections in the time signals [33]. For the signals shown in Fig. 11, the coefficient of determination $R^2$ is 0.996 and 0.962, respectively. For the nRMSE, values of 0.018 and 0.050 are obtained.

For the entire group of 175 welds, the results of the down-sampled envelope curves are plotted against each other in the correlation plot in Fig. 15.

There seems to be a good match between the two signals with some minor deviations caused by small offsets. Table 6. shows the statistical results for the different test series. There is a good agreement between the groups with a range for the coefficient of determination $R^2$ from 0.982 to 0.991. The nRMSE is very small with values ranging from 0.026 to 0.048. Only the contaminated group is slightly worse. This could be caused by a high inconsistency of the welds themselves.

Analyzing the amplitude curves for the higher harmonic frequencies leads to different results. While the signals seem

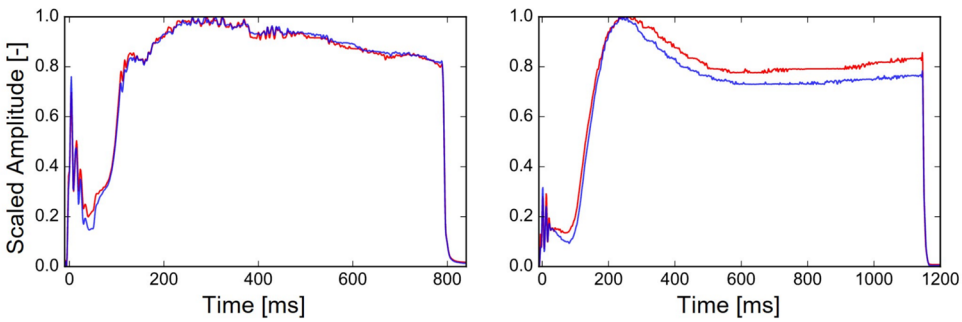



**Fig. 14** Standardized envelope curves of the sensor signals of shear force sensor (red) and vibrometer sensor (blue): left: best result in reference group ($R^2$: 0.996); right: worst result in reference group ($R^2$: 0.962)

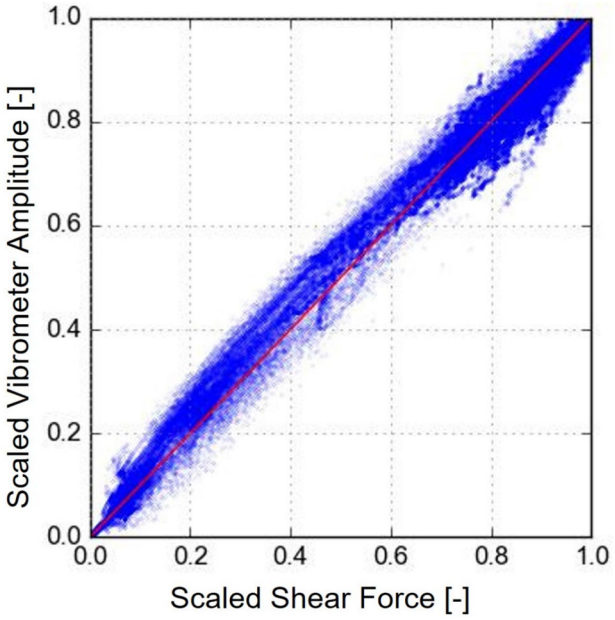



**Fig. 15** Correlation plot of vibrometer and shear force for all welds

**Table 6** Overview of results of correlation between envelopes at 20–21 kHz

| Test series | Material | Number of tests | $R^2$ [-] | nRMSE [-] |
|---|---|---|---|---|
| R | Reference (foil clean) | 35 | 0.989 | 0.027 |
| C | Chemically cleaned | 35 | 0.987 | 0.029 |
| H | Hardness | 35 | 0.991 | 0.026 |
| F | Contamination | 35 | 0.983 | 0.048 |
| X | Without clamping | 35 | 0.982 | 0.029 |
| | **Overall** | **175** | **0.986** | **0.032** |

to correlate very well at a frequency range of 60 – 61 kHz (see Fig. 16 (right)) with a $R^2$ of 0.947 and a nRMSE of 0.053, the correlation at the second harmonic at a frequency range of 40 – 41 kHz is not very promising (see Fig. 16 (left)) with a $R^2$ of 0.519 and a nRMSE of 0.154. This could be due to the vertical distance of ~ 38 mm between the vibrometer and shear force sensor, resulting in poor correlation of the signals in the second harmonic. In addition, a certain inconsistency in the signals is also possible, as the shear force sensor, for example, does not output a perfect 1D signal due to its design. This can also be seen in Fig. 13 where the signal-to-noise-ratio of the second harmonic is worse than that of the third harmonic.

As the evaluation of the working frequency range for the vibrations at the horn and anvil as well as in the electrical output power of the generator has proven to be sufficient in the practical analysis for quality monitoring [8, 11, 14], the reduction of the correlation between laser and shear force sensor for the higher frequency range is not considered to be critical.

## 4 Summary and outlook

This paper presented and successfully implemented a design and validation process for an anvil with integrated, piezoelectric-based shear force sensors for USMW. The dynamic force curve that can be measured during the welding process correlates excellently with a reference amplitude signal that can be recorded by a vibrometer on the anvil. The correlation of the measurement data from 175 welding tests with five different welding conditions, results in a mean coefficient of determination $R^2$ ~ 0.986 with an error measure nRMSE of ~ 0.032 for amplitude envelopes determined from band-pass-filtered signals in the range of the operating frequency of ~ 20 kHz.

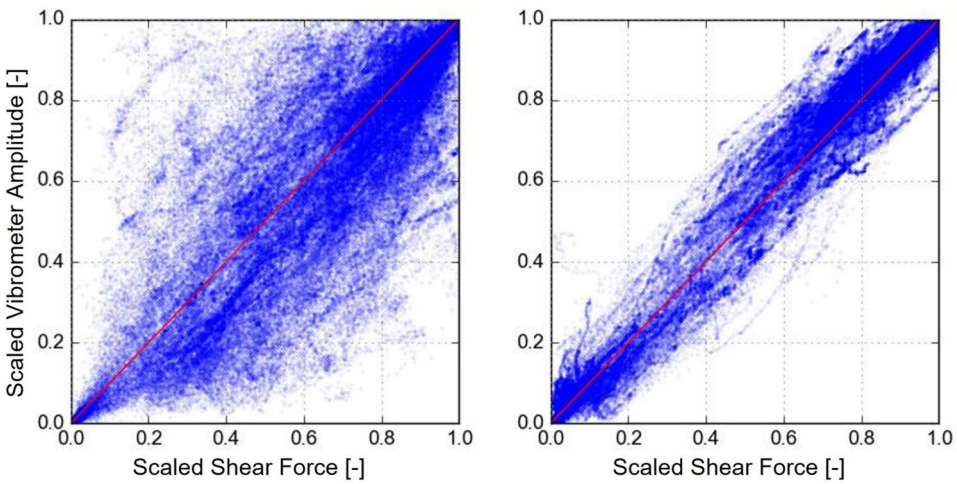



**Fig. 16** Correlation of shear force signal and vibrometer signal at the higher harmonics: 40 kHz (left) and 60 kHz (right)

The shear force sensor system is therefore a promising alternative to vibrometers for capturing high-frequency amplitude, frequency, and phase information at the anvil during USMW. The investigations show that a robust installation in a larger test setup is possible. The quantification of the determined shear force signal should still be used with caution since an increase compared to the quasi-static signal can be determined. The exact determination of this increase is challenging, since in particular the dynamic damping present during the process in the individual components of the anvil structure is unknown and still under investigation.

Future research should investigate whether the methodology can be transferred to other anvil designs closer to industrial production standards and what loss of process performance can be expected because of reduced anvil stiffness. In addition to evaluating further data pre-processing variants, we also plan to investigate the mounting of the sensors in force bypass to increase the anvil stiffness, although this must be expected to result in reduced sensor sensitivity.

**Author contribution** All authors contributed to the study conception and design. Component design, simulation, material preparation, and data collection were performed by E. Helfers. Data analysis and correlation were performed by O. Stockemer and E. Helfers. The first draft of the manuscript was written by E. Helfers and O. Stockemer. All authors commented on previous versions of the manuscript. All authors read and approved the final manuscript.

**Funding** Open Access funding enabled and organized by Projekt DEAL. Funded by the Deutsche Forschungsgemeinschaft (DFG—German Research Foundation) under Grant Number 520475171 "Hybrid Process Prediction for Ultrasonic Metal Welding – Pro$^{2MUSS}$".

**Data availability** Data will be made available on reasonable request by the corresponding author.

## Declarations

**Competing interests** The authors declare no competing interests.

**Open Access** This article is licensed under a Creative Commons Attribution 4.0 International License, which permits use, sharing, adaptation, distribution and reproduction in any medium or format, as long as you give appropriate credit to the original author(s) and the source, provide a link to the Creative Commons licence, and indicate if changes were made. The images or other third party material in this article are included in the article's Creative Commons licence, unless indicated otherwise in a credit line to the material. If material is not included in the article's Creative Commons licence and your intended use is not permitted by statutory regulation or exceeds the permitted use, you will need to obtain permission directly from the copyright holder. To view a copy of this licence, visit http://creativecommons.org/licenses/by/4.0/.

## References

1. Gallego-Juárez JA, Graff KF, Lucas M, editors. Power ultrasonics: applications of high-intensity ultrasound. Second edition. Oxford: Woodhead Publishing, 2022 [https://doi.org/10.1016/C2019-0-00783-2]
2. Wodara, J., Adam, T. Ultraschallfügen und -trennen.: Band 1 der Grundlagen der Fügetechnik. Düsseldorf: DVS Verlag, 2004, ISBN: 3–87155–212–7.
3. Balz I. Prozessanalyse der thermo-mechanischen Vorgänge während der Verbindungsbildung beim Metall-Ultraschallschweißen // Analysis of thermo-mechanical processes during the bond formation in ultrasonic metal welding. 1. Auflage. Düren: Shaker 2020 [https://doi.org/10.18154/RWTH-2020-08744]
4. Helfers E, Müller FW, Schiebahn A, Reisgen U (2024) Influence of surface condition of copper sheets on ultrasonic metal welding. J Adv Join Process 9:100204. https://doi.org/10.1016/j.jajp.2024.100204
5. Müller FW, Chen C-Y, Schiebahn A, Reisgen U (2023) Application of electrical power measurements for process monitoring in ultrasonic metal welding. Weld World 67(2):395–415. https://doi.org/10.1007/s40194-022-01428-9
6. Vries E de. Mechanics and mechanisms of ultrasonic metal welding: the Ohio State University, 2004 [cited accessed on 2025 January 26] Available from: URL: http://rave.ohiolink.edu/etdc/view?acc_num=osu1078415529.
7. Müller FW, Schiebahn A, Reisgen U (2022) Quality prediction of disturbed ultrasonic metal welds. J Adv Join Process 5:100086. https://doi.org/10.1016/j.jajp.2021.100086
8. Müller FW, Zhao H, Schiebahn A, Reisgen U (2024) Joint quality assessment of ultrasonic metal welded parts by fracture surface evaluation. Metals 14(8):892. https://doi.org/10.3390/met14080892
9. Meng Y, Lu K-C, Dong Z, Li S, Shao C (2023) Explainable few-shot learning for online anomaly detection in ultrasonic metal welding with varying configurations. J Manuf Process 107:345–355. https://doi.org/10.1016/j.jmapro.2023.10.047
10. Gester A, Sprigode T, Wagner G (2024) Publisher correction: novel approach for in-line process monitoring during ultrasonic metal welding of dissimilar wire/terminal joints based on the thermoelectric effect. Weld World 68(12):3235–3236. https://doi.org/10.1007/s40194-024-01860-z
11. Müller FW, Mirz C, Weil S, Schiebahn A, Corves B, Reisgen U (2023) Weld quality characterization by vibration analysis for ultrasonic metal welding processes. J Adv Join Process 8:100149. https://doi.org/10.1016/j.jajp.2023.100149
12. Gester A. Prozesscharakterisierung des Kompaktierungsverhaltens metall-ultraschallgeschweißter Verbindungen aus Cu-ETP und Aluminium-Fahrzeugleitungen. Chemnitz University of Technology 2024 [https://doi.org/10.60687/2024-0108]
13. Abi Raad E, Müller FW, Reisgen U, Vorländer M (2023) Experimental setup for laser vibrometry measurements of the vibrating horn in ultrasonic metal welding. inter noise 265(5):2549–2560. https://doi.org/10.3397/IN_2022_0358
14. Schwarz EB, Bleier F, Guenter F, Mikut R, Bergmann JP (2022) Improving process monitoring of ultrasonic metal welding using classical machine learning methods and process-informed time series evaluation. J Manuf Process 77:54–62. https://doi.org/10.1016/j.jmapro.2022.02.057
15. Raad EA, Balz I, Reisgen U, Vorländer M. Investigation of the applicability of acoustic emission and vibration analysis to describe the thermo-mechanical mechanism during ultrasonic metal welding, 2019 [https://doi.org/10.18154/RWTH-CONV-239778]

16. Wu Y, Meng Y, Shao C (2022) End-to-end online quality prediction for ultrasonic metal welding using sensor fusion and deep learning. J Manuf Process 83:685–694. https://doi.org/10.1016/j.jmapro.2022.09.011
17. Lee D, Cai W (2017) The effect of horn knurl geometry on battery tab ultrasonic welding quality: 2D finite element simulations. J Manuf Process 28:428–441. https://doi.org/10.1016/j.jmapro.2017.04.009
18. Taylor JR. Classical mechanics. [Nachdr.] Sausalito, Calif.: University Science Books, 2005, ISBN: 189138922X.
19. Dobmann G, Paul M, Eifler D, Faßbender S, inventors; Fraunhofer-Gesellschaft zur Förderung der angewandten Forschung eV, München, assignee. Vorrichtung zum Schweißen mit Ultraschall: Patentschrift 2000; DE000019810509C2.
20. Liesegang M. Kontinuierliches Ultraschallschweißen ebener und rohrförmiger Titan/CFK-Verbindungen // Kontinuierliches Ultraschallschweißen ebener und rohrförmiger Titan/CFK-Verbindungen – Sonotroden, Prozessentwicklung und Verbundeigenschaften. DissertationTechnische Universität Kaiserslautern 2021 [https://doi.org/10.26204/KLUEDO/6290]
21. Jahn R, Cooper R, Wilkosz D (2007) The effect of anvil geometry and welding energy on microstructures in ultrasonic spot welds of AA6111-T4. Metall Mater Trans A 38(3):570–583. https://doi.org/10.1007/s11661-006-9087-0
22. Littmann W. Piezoelektrische, resonant betriebene Ultraschall-Leistungswandler mit nichtlinearen mechanischen Randbedingungen. Paderborn: Heinz-Nixdorf-Inst, 2003, ISBN: 3935433336.
23. DIN EN 13599:2014-12, Kupfer und Kupferlegierungen_- Platten, Bleche und Bänder aus Kupfer für die Anwendung in der Elektrotechnik; Deutsche Fassung EN_13599:2014: Copper and copper alloys - Copper plate, sheet and strip for electrical purposes; German version EN 13599:2014. Berlin: DIN Media GmbH [https://doi.org/10.31030/2251682]
24. Hottinger Baldwin Messtechnik GmbH. CSW - Piezoelectric force washer for shear forces: Data sheet, 2024 [cited 2025 January 26] Available from: URL: https://www.hbm.com/fileadmin/mediapool/hbmdoc/technical/B04819.pdf.
25. Dresig H, Holzweißig F. Maschinendynamik. 12. Aufl. 2016. Berlin, Heidelberg: Springer Berlin Heidelberg 2016 [https://doi.org/10.1007/978-3-662-52713-9]
26. Kistler Group. Instruction Manual: SlimLine Sensors (SLS) for Shear Force Type 9143B… to 9147B…, 2010 [cited 2025 January 26] Available from: URL: https://kistler.cdn.celum.cloud/SAPCommerce_Download_original/002-285e.pdf.
27. Kleckers, Thomas - Product Manager Force HBK 20.12.2024 – Additional product information on CSW, 2024; phone call.
28. Stahlschlüssel-Taschenbuch: Wissenswertes über Stähle. 19. Aufl. Marbach/N.: Verl. Stahlschlüssel Wegst 2001, ISBN: 3922599168.
29. Cremer L, Heckl M (1988) Structure-borne sound: structural vibrations and sound radiation at audio frequencies. Second Edition. Berlin, Heidelberg, s.l.: Springer Berlin Heidelberg 1988 [https://doi.org/10.1007/978-3-662-10121-6]
30. Adams RD (1972) The damping characteristics of certain steels, cast irons and other metals. J Sound Vib 23(2):199–216. https://doi.org/10.1016/0022-460X(72)90560-3
31. Pedregosa F, Varoquaux G, Gramfort A, et al (2011) Scikit-learn: Machine Learning in Python, 2011. Available from: URL: http://arxiv.org/pdf/1201.0490.
32. Daubechies I, Lu J, Wu H-T (2011) Synchrosqueezed wavelet transforms: an empirical mode decomposition-like tool. Appl Comput Harmon Anal 30(2):243–261. https://doi.org/10.1016/j.acha.2010.08.002
33. Fahrmeir L, Heumann C, Künstler R, Pigeot I, Tutz G. (2023) Statistik: Der Weg zur Datenanalyse. 9., überarbeitete und ergänzte Auflage. Berlin, Heidelberg: Springer Spektrum [https://doi.org/10.1007/978-3-662-67526-7]

**Publisher's Note** Springer Nature remains neutral with regard to jurisdictional claims in published maps and institutional affiliations.